Chen *et al.*
Chinese Journal of Mechanical Engineering (2023) 36:66
https://doi.org/10.1186/s10033-023-00890-w

Chinese Journal of Mechanical Engineering

ORIGINAL ARTICLE

Open Access

Generation and Evolution of Cavitation Bubbles in Volume Alternate Cavitation (VAC)

Shangshuang Chen[1], Yun Wang[1*], Fuzhu Li[1], Shenwei Xue[1], Zhenying Xu[1], Chao Yu[1] and Kun Zhang[1]

Abstract

Cavitation generation methods have been used in multifarious directions because of their diversity, and numerous studies and discussions have been conducted on cavitation generation methods. This study aims to explore the generating mechanism and evolution law of volume alternate cavitation (VAC). In the VAC, liquid water is placed in an airtight container with a variable volume. As the volume alternately changes, the liquid water inside the container continues to cavitate. Then, the mixture turbulence model and in-cylinder dynamic grid model are adopted to conduct computational fluid dynamics simulation of volume alternate cavitation. In the simulation, the cloud images at seven heights on the central axis are monitored, and the phenomenon and mechanism of height and eccentricity are analyzed in detail. By employing the cavitation flow visualization method, the generating mechanism and evolution law of cavitation are revealed. The synergistic effects of experiments and high-speed camera capturing confirm the correctness of the simulation results. In the experiment, the volume change stroke of the airtight container is set to 20 mm, the volume change frequency is 18 Hz, and the shooting frequency of the high-speed camera is set to 10000 FPS. The experimental results indicate that the position of the cavitation phenomenon has a reasonable law during the whole evolution cycle of the cavitation cloud. Also, the volume alternation cycle corresponds to the generation, development, and collapse stages of cavitation bubbles.

Keywords Cavitation generation method, Volume alternate cavitation (VAC), Generating mechanism, Evolution law, Computational fluid dynamics (CFD), Cavitation flow visualization (CFV)

1 Introduction

Nowadays, the cavitation generation method mainly includes hydrodynamic cavitation, ultrasonic cavitation and laser-induced cavitation, and its application covers cleaning, surface treatment, cavitation molding, environmental protection and renewable, etc.

The traditional cavitation generation method has been investigated by many researchers. The theory and application of hydrodynamic cavitation [1–3], an important cavitation generation method, have received much research attention. A systematic and detailed study on hydrodynamic cavitation for disinfection has been conducted [4]. The energy release of the cavitation phenomenon and its mechanism are described, and the effectiveness, economy and applicability of hydrodynamic cavitation disinfection have been confirmed. Pooja et al. [5] explored the degradation of benzene in wastewater by hydrodynamic cavitation in combination with air. Via the experimental study of inlet pressure, thermal conductivity, treatment duration and airflow ratio, the optimal parameter setting for degrading benzene is obtained. Panda et al. [6] provided a detailed report on the development trend and practical application of hydrodynamic cavitation in recent years, and they pointed out future development directions regarding specific deficiencies. Besides hydrodynamic cavitation, many other cavitation generation methods have been investigated. The effect of viscosity reduction is studied through the synergistic

*Correspondence:
Yun Wang
wangyun@ujs.edu.cn
[1] School of Mechanical Engineering, Jiangsu University, Zhenjiang 212013, China

effect of ultrasonic cavitation [7] and heterogeneous catalysts [8]. Shen et al. [9] applied ultrasonic cavitation to medicine and investigated the influences of different parameters in ultrasonic cavitation on inducing apoptosis of tumor cells. Abhinav et al. [10] explored the impact force of a single bubble rupture under the combination of laser-induced cavitation [11, 12] and acoustic cavitation. Pello et al. [13] discussed the combination of ultrasonic cavitation and ozone to treat wastewater, and the treated wastewater satisfy the standards for microbial disinfection of drinking water. After research, these traditional cavitation generation methods can be applied to life and production [14].

Although cavitation research has a long history, the research on the mechanism of cavitation generation methods and cavitation evolution law has never been interrupted. Sun et al. [15] analyzed the cavitation mechanism and development process of the cavitation flow field located on the rotor and stator, and it was found that the shape and size of the vortex cavitation depended on the compression effect generated by the interaction. A new type of rotary hydrodynamic cavitation generator has been studied and applied to the refinement of cellulose pulp, and the generator is proven to be more economical and effective than conventional methods [16, 17]. Chen et al. [18, 19] designed experimental equipment for cavitation generated by negative pressure, investigated the erosion effect [20] of negative pressure cavitation on the material removal rate and surface roughness, and proposed a type of cavitation water-suction polishing without grinding conditions to remove materials through the green manufacturing method. Among them, the cavitation flow visualization (CFV) [15, 17, 21–23] method was used by researchers to capture the cavitation phenomenon. The dynamic evolution law of the cavitation cloud of a submerged water jet was obtained by visualization of cavitation flow [24]. Cai [25] investigated the occurrence and evolution of cavitation in capillary tubes under temperature alternation, and made a corresponding theoretical analysis and experimental discussion. In evidence, to break through the limitations of traditional cavitation generation methods, novel cavitation generation methods emerge endlessly.

This paper proposes a new cavitation generation method called volume alternate cavitation (VAC). Different from traditional cavitation generation methods, the mechanism of VAC is based on the change in volume of the airtight container to form a low-pressure environment whose pressure is lower than the saturation vapor pressure of the liquid phase, and then the cavitation bubbles are formed in the low-pressure environment, and finally the cavitation bubbles are broken by high-pressure extrusion [26]. Due to the volume changes in the airtight container, cavitation bubbles are constantly generated and broken. However, cavitation bubbles rupture [27, 28] will generate extremely huge energy, which helps to polish and strengthen the wall surface [29, 30], especially for the inner surface of complex cavities. Additionally, VAC can also be used for rapid emulsion manufacturing, cavitation cleaning [31, 32] and other applications. The advantages of this cavitation generation method are distinct, e.g. the method of VAC is simple and easy to operate, and the device of VAC is environmentally friendly and energy saving. Moreover, this study can guide the application and design of VAC in the future. Cavitation is caused by local pressure below the saturated vapor pressure of the liquid, but this is only the mechanism of cavitation formation [33], not the cavitation generation method. Similar to hydrodynamic cavitation, ultrasonic cavitation depends on this mechanism. However, they are different methods of cavitation generation methods, with different processes. For the new cavitation generation methods, this paper studied the formation position and evolution of cavitation bubbles in VAC.

2 Experimental Facility

As shown in Figure 1, an experimental platform was constructed to meet the experimental requirements. The experimental platform consists of a cavitation generator, a shooting device, a motor drive device, a control terminal and supports. The cavitation generator is an airtight container made of assembled parts, which can meet the requirement that there is only water in the airtight container without excess air pressure. The sample in the cavitation generator has a hole with a depth of 30 mm and a diameter of 4 mm inside. The shooting device is composed of a high-speed camera, a high-power LED light, and reflective glass. In the filming process, high-speed cameras are placed in front of the experimental facility, with the LED light as a background light. The shadow imaging method [24] is adopted to capture the phenomenon of the VAC. To reflect the complete period of the experimental phenomena in detail, the time interval of the high-speed camera is set to 10000 FPS. The motor drive device is employed to drive the reciprocating movement of the push rod, and then realize the reciprocating movement of the piston inside the cavitation generator, to meet the conditions of generating VAC. Figure 2 shows the schematic diagram of the device.

As shown in Figure 2, the experimental details can be summarized as follows:

(1) The environment for cavitation is an airtight container, which can well avoid the exchange of gas with the outside.

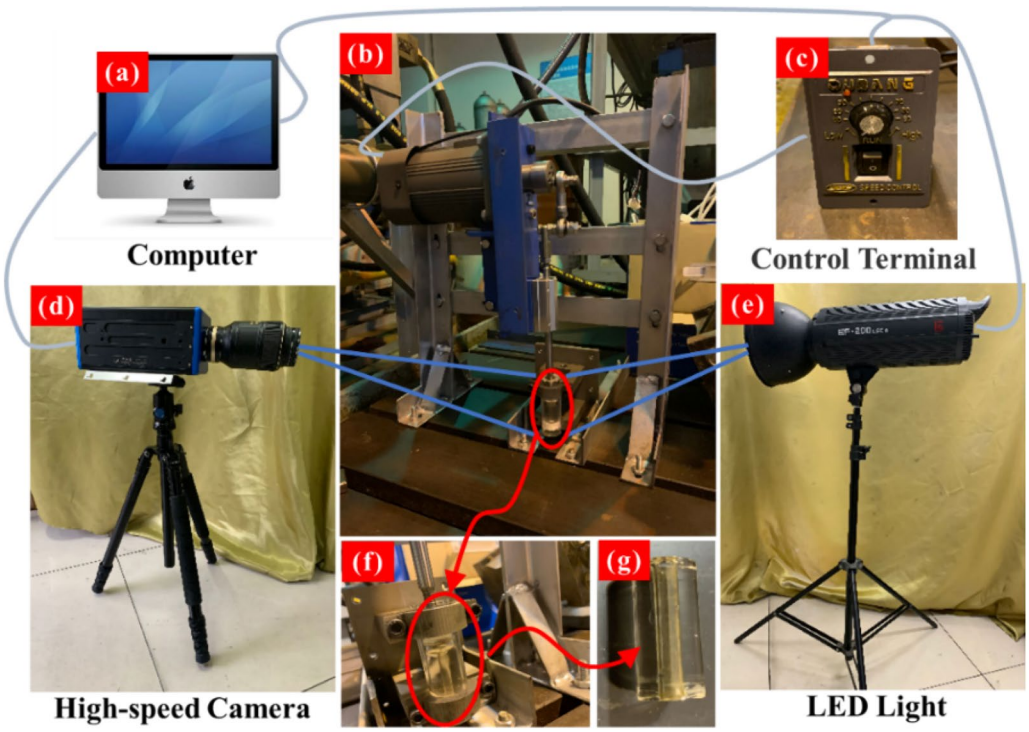

Figure 1 Experimental platform: (**a**) Computer, (**b**) Motor drive device, (**c**) Control terminal, (**d**) High-speed camera, (**e**) LED light, (**f**) Cavitation generator, (**g**) Sample

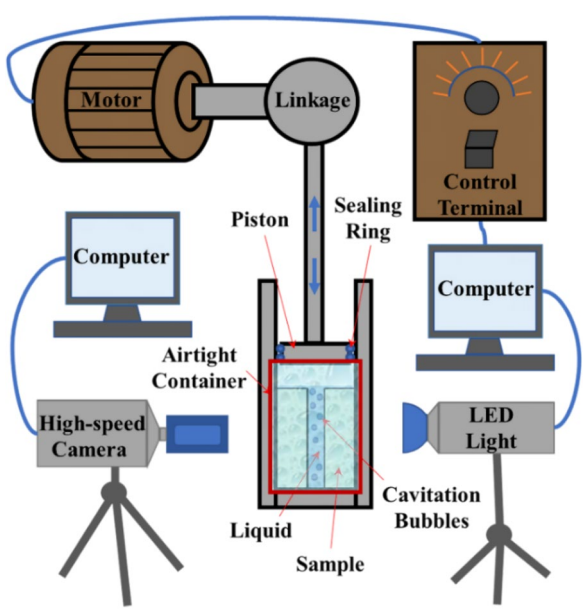

Figure 2 Schematic diagram of the VAC

(2) The airtight container is a cylinder that consists of three faces: the upper surface, the side surface and the bottom surface. Inside the container sits a cylindrical sample with a small hole.
(3) The side and the bottom surface of the airtight container are fixed, and the upper surface is essentially the bottom surface of the piston.
(4) The piston has two vital functions. One function is the sealing ring around the piston to ensure that the airtight container is sealed, the other function is that the piston can move up and down under the drive of the motor and linkage to realize the volume alternation of the airtight container.

3 Numerical Analysis

3.1 Theory

3.1.1 Mixture Model

The Mixture model in computation fluid dynamics (CFD) can be used for two-phase or multiphase flow calculation. The model allows interphase penetration, i.e. that is,

the sum of the volume fraction of each phase in each grid cell can be any value between 0 and 1. The model also allows for phase slip, indicating that each phase can have different velocities. Through analysis, the mixture model is suitable for the numerical analysis of this study, and its momentum conservation equation is:

$$\frac{\partial}{\partial t}(\rho_m \boldsymbol{v_m}) + \nabla(\rho_m \boldsymbol{v_m}\boldsymbol{v_m}) = -\nabla p + \nabla[\mu_m(\nabla \boldsymbol{v_m} + \nabla \boldsymbol{v_m}^{\mathrm{T}})] + \rho_m \boldsymbol{g} + \boldsymbol{F} - \nabla\left(\sum\nolimits_{k=1}^{n} \alpha_k \rho_k \boldsymbol{v}_{dr,k} \boldsymbol{v}_{dr,k}\right), \tag{1}$$

where, n is the number of phases, $\boldsymbol{F}$ is the volume force, μ_m is the viscosity of the mixed phase:

$$\mu_m = \sum\nolimits_{k=1}^{n} \alpha_k \mu_k, \tag{2}$$

and $\boldsymbol{v}_{dr,k}$ is the drift velocity of the quadratic term.

$$\boldsymbol{v}_{dr,k} = \boldsymbol{v}_k - \boldsymbol{v}_m. \tag{3}$$

3.1.2 Dynamic Mesh Model

Regarding the dynamic mesh, the integral form of the general scalar in the conservation equation is denoted as Φ . Under the premise of any controllable volume V, the boundary motion of the mesh can be expressed as:

$$\frac{d}{\mathrm{d}t}\int_V \rho\Phi \mathrm{d}V + \int_{\partial V} \rho\Phi\left(\boldsymbol{u} - \boldsymbol{u}_g\right)\mathrm{d}\boldsymbol{A} = \int_{\partial V} \Gamma\nabla\Phi\partial\mathrm{d}\boldsymbol{A} + \int_V S_\Phi \mathrm{d}V, \tag{4}$$

where ρ is the density of the fluid, $\boldsymbol{u}$ is the velocity vector, $\boldsymbol{u}_g$ is the moving velocity of the moving mesh, Γ is the diffusion coefficient, and S_Φ is the source term of Φ. Here, ∂V is used to express the boundary of the controlled volume V.

3.2 Numerical Analysis of the Complete Period

To reveal the specific mechanism of VAC, the reciprocating motion of the piston is exploited to control the alternate change of volume. Therefore, this study takes an alternate change of volume as the basis for simulation. The height of the inner hole in the sample was equally divided into six sections, with a total of seven heights, and the change of the gas phase volume fraction was monitored at the seven heights monitored within a motion period. Figure 3 shows the initial simulation model and the distribution of different heights in the piston's inner hole.

3.2.1 Gas Phase Volume Fraction Distribution Cloud Nephogram

The volume variation in this study is based on the motion controllability of the upper interface. In the simulation process, the upper interface takes a motion frequency of 18 Hz and a motion stroke of 20 mm to monitor the specific situation of the gas phase volume fraction within a cycle and make the corresponding simulation cloud map. Figure 4 shows the cloud nephogram of the gas phase volume fraction at seven heights in the inner hole.

3.2.2 Influence of Height on Cavitation Formation

Figure 5 demonstrates the data diagram of gas phase volume distribution at different heights along the central axis of the inner hole with time variation. It can be seen that the gas phase volume fraction varies constantly over time at each height.

Wherein, the height of 0 represents the change rule of the gas phase volume fraction at the bottom of the hole. It is found that the gas phase volume fraction at the bottom of the hole is high at the beginning and then decreases continuously. The reason for this change is that in the initial process, the liquid will be attached to the piston due to the tension, and the upward movement of the piston will drive the liquid upward. There will be a low-pressure area at the bottom of the liquid. When the pressure of

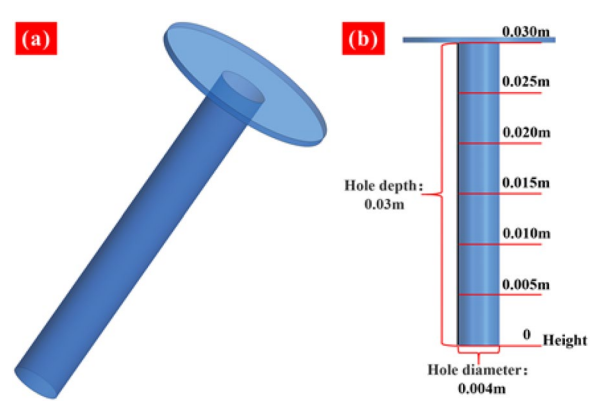

Figure 3 Simulation model

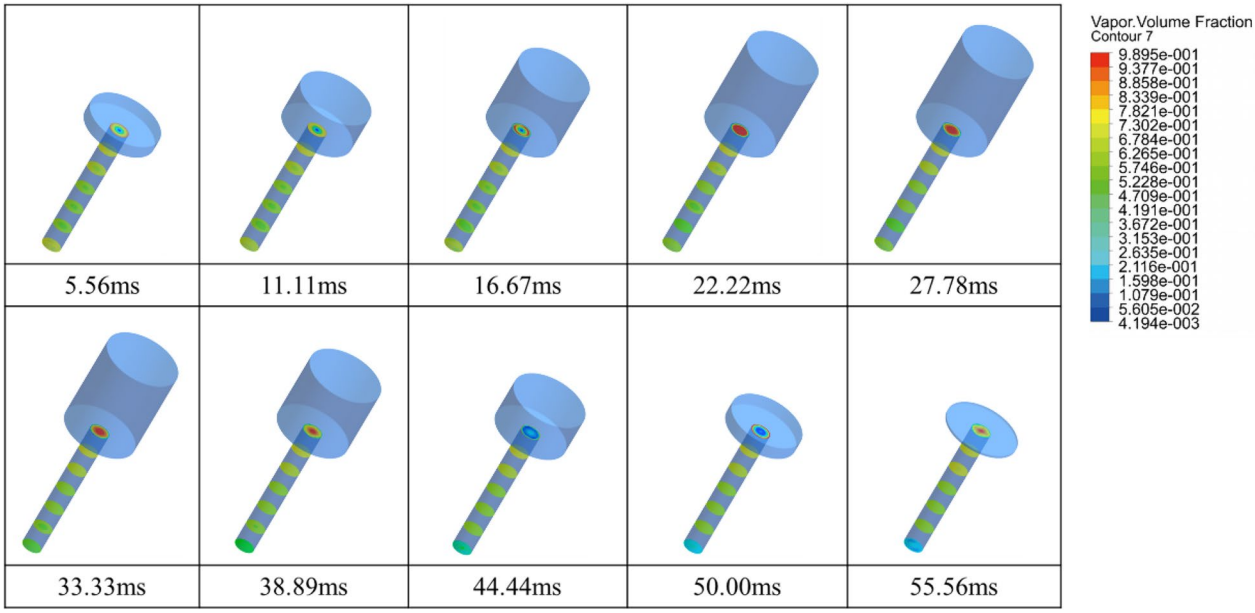

Figure 4 Periodic cloud map

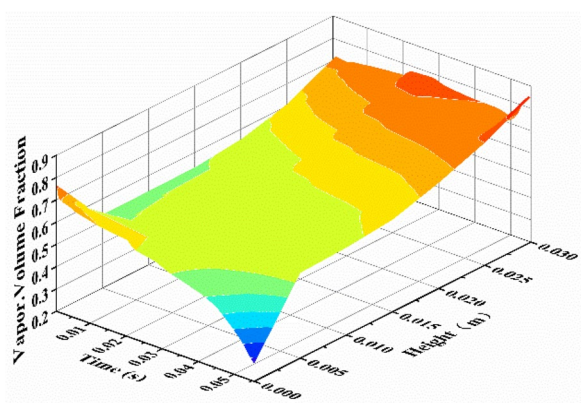

Figure 5 Gas phase volume distribution at different heights along the central axis of the inner hole with time

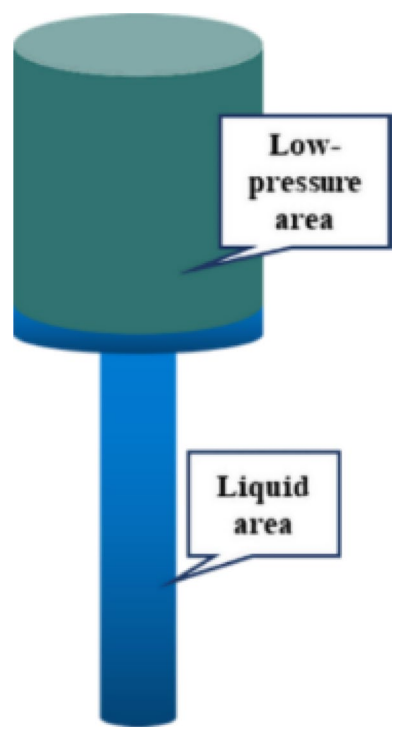

Figure 6 Schematic diagram of low-pressure zone in vacuum-like environment

the low-pressure area is lower than the saturated vapor pressure of the liquid, the liquid will be transformed into gas. After the initial process, due to gravity, the liquid attached to the piston separates from the piston and begins to deposit downward. Meanwhile, the generated gas, which is less dense than the liquid, floats upward through the liquid, leading to a declining volume fraction of the gas phase at the bottom of the hole.

The height of 0.03 m represents the situation of the gas phase volume fraction on the upper surface. It can be seen from Figure 5 that the gas phase volume fraction on the upper surface is more than that at other heights of the inner hole. The reason for this phenomenon is summarized below: when the piston is moving, the liquid is always inside the hole due to gravity, so there is a low-pressure area like a vacuum on the upper surface, as

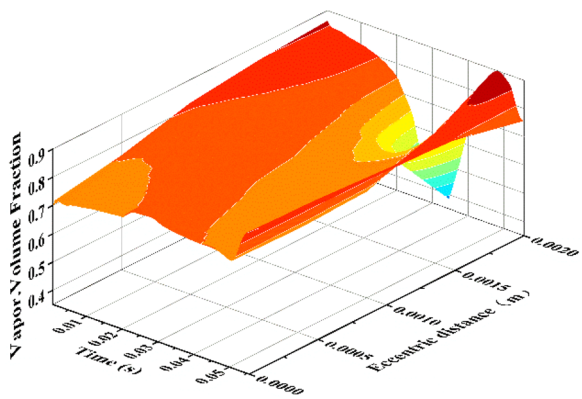

Figure 7 Variation of gas phase volume fraction with different eccentricity on the upper surface over time

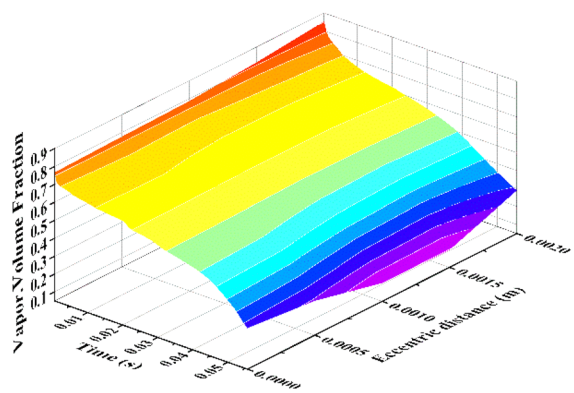

Figure 8 Variation of gas phase volume fraction with different eccentricity at the bottom surface over time

illustrated in Figure 6. The pressure in this low-pressure area is much lower than the saturated vapor pressure of the liquid, causing the liquid on the upper surface to undergo a violent phase transition, i.e. constantly changing from liquid to gas. The gas phase volume fraction on the upper surface appears at the middle stage and the last stage of the piston movement cycle. The two peak values of gas phase volume fraction appear in the middle stage and the final stage of the piston motion cycle, respectively. The reason for the peak in the middle stage is that at this time, when the piston moves to the limit stroke, the liquid phase in the inner hole is transformed into the gas phase by the most amount, and the generated gas is mostly filled in the vacuum-like low pressure area above the liquid. As the generated gas increases, the liquid level will decline, leading to a higher fraction volume of the gas phase on the upper surface. The reason for the peak in the final stage is that the piston begins to return to its initial height. Due to the excessive speed, the gas in the vacuum-like low-pressure area has been pushed back into the hole before it is converted into liquid, resulting in a sharp increase in the gas phase volume fraction at this time.

3.2.3 Influence of Eccentricity on Cavitation Formation

Regarding the above results, this study explored the upper surface and bottom surface of the inner hole, and analyzed the relationship between the gas volume fraction in these two planes and the eccentricity (the distance from the central axis of the inner hole). The processing results are shown in Figures 7 and 8.

Figure 7 shows the variation of gas phase volume fraction with different eccentricities on the upper surface over time. It can be seen from the figure that the gas phase volume fraction is generally maintained at a relatively high level of above 0.7. However, when the eccentricity is 0.002 m and the time is 0.0034 s, the gas phase volume fraction decreases sharply to less than 0.4. The reason for this charge is summarized as follows: at 0.0034 s, the piston moves to the limit stage of stroke. At this time, the velocity of the piston is close to zero. Meanwhile, the conversion rate from the liquid phase to the gas phase reaches a very low level, and the conversion from the gas phase to the liquid phase begins. The area with an eccentricity of 0.002 m belongs to the near-wall surface, and the newly generated liquid phase will be preferentially adsorbed to the wall surface, leading to a sharp decrease in the volume fraction of the gas phase.

Figure 8 shows the variation of gas phase volume fraction with different eccentricities at the bottom surface over time. It can be observed from the figure that the volume fraction of the gas phase decreases over time, and different eccentricity has little effect on the volume fraction of the gas phase.

4 Results and Discussion

4.1 Formation Stage of Cavitation Bubbles

To verify the correctness of the simulation results, a series of experiments were carried out, and a high-speed camera was used to capture the phenomenon. Meanwhile, the method of CFV is used flexibly here. Figure 9 shows the cavitation situation in the hole when the volume just starts to increase. As shown in Figure 9, as the volume increases, the cavitation bubbles are generated at a height of 0, and there are a large number of cavitation bubbles on the upper surface, i.e., the primary stage of cavitation, which is consistent with the explanation given in Figure 5 that cavitation occurs on the bottom and the upper surface. Figure 10 shows the schematic diagram of the initial generation of cavitation bubbles at the bottom surface. The cavitation generation phase reveals the process of cavitation bubbles from nothing to existence, which confirms the feasibility of VAC.

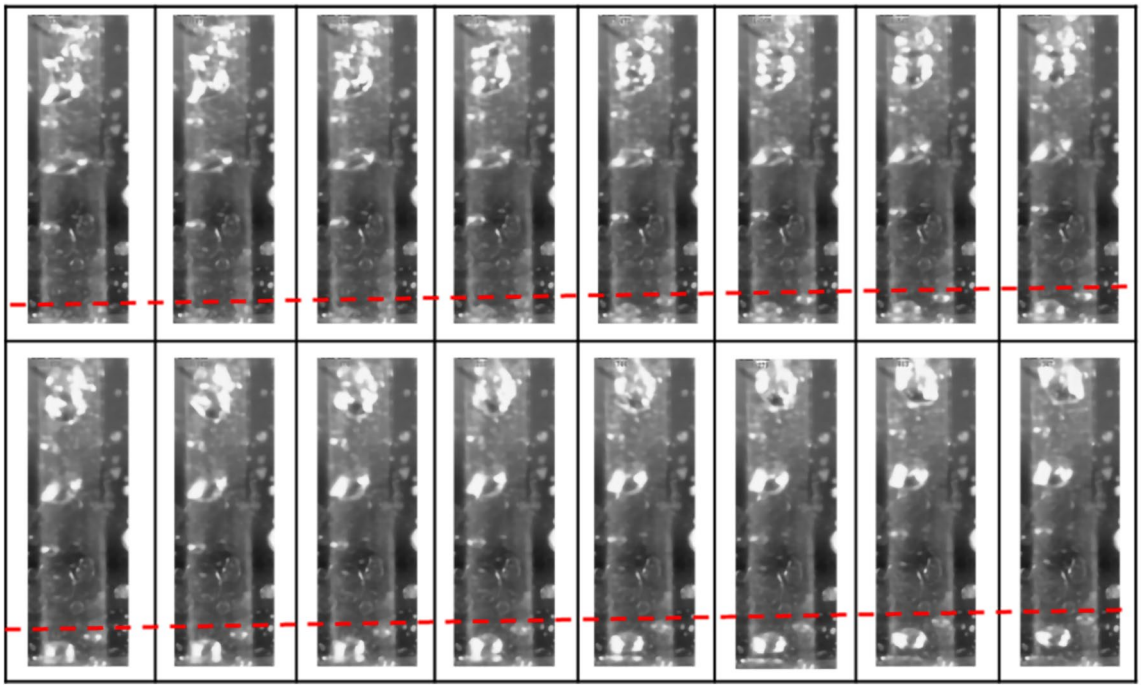

Figure 9 Diagram of cavitation bubble formation

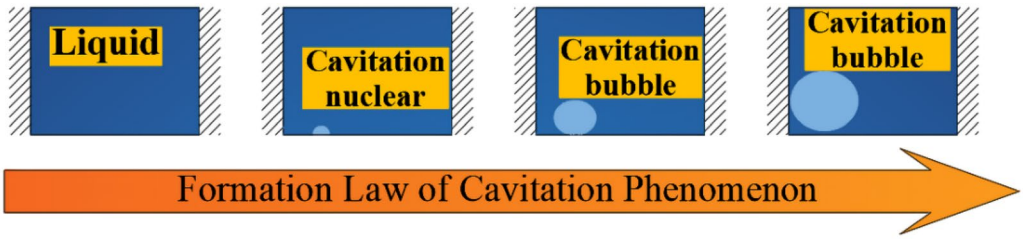

Figure 10 Schematic diagram of cavitation bubble formation

4.2 Development Stage of Cavitation Bubbles

As the volume continues to increase, the cavitation cloud begins to evolve further. As shown in Figure 11, the rise of the piston drives cavitation bubbles near the upper surface to move upward. Meanwhile, the cavitation cloud separation phenomenon appears considering that the bubbles farther away from the upper interface tend to move downward. The violent cavitation reaction at the upper interface also corresponds to the explanation given in Figure 5. In the process of separation, the large bubble is torn [25] and a new small bubble begins to form.

4.3 Collapse Stage of Cavitation Bubbles

Cavitation bubble collapse mainly occurs at the end of the volume alternation cycle, i.e., the piston returns to the liquid level again. As shown in Figure 12, when the piston moves to the end of a period, many gas phases appear on the upper surface of the liquid, which is consistent with the interpretation of the simulation results. However, cavitation collapse is particularly significant at this stage, with large cavitation bubbles collapsing into a great number of small cavitation bubbles. Figure 13 is a schematic diagram of cavitation bubble collapse.

During VAC, the evolution of cavitation bubbles in the liquid depends on the reciprocating movement of the piston (i.e., volume alternation). The container is completely filled with liquid at the initial state, and cavitation bubbles are generated when the container volume becomes larger. When the container volume becomes smaller, the bubbles will be compressed by the generated high pressure to collapse (since there is no extra volume to store

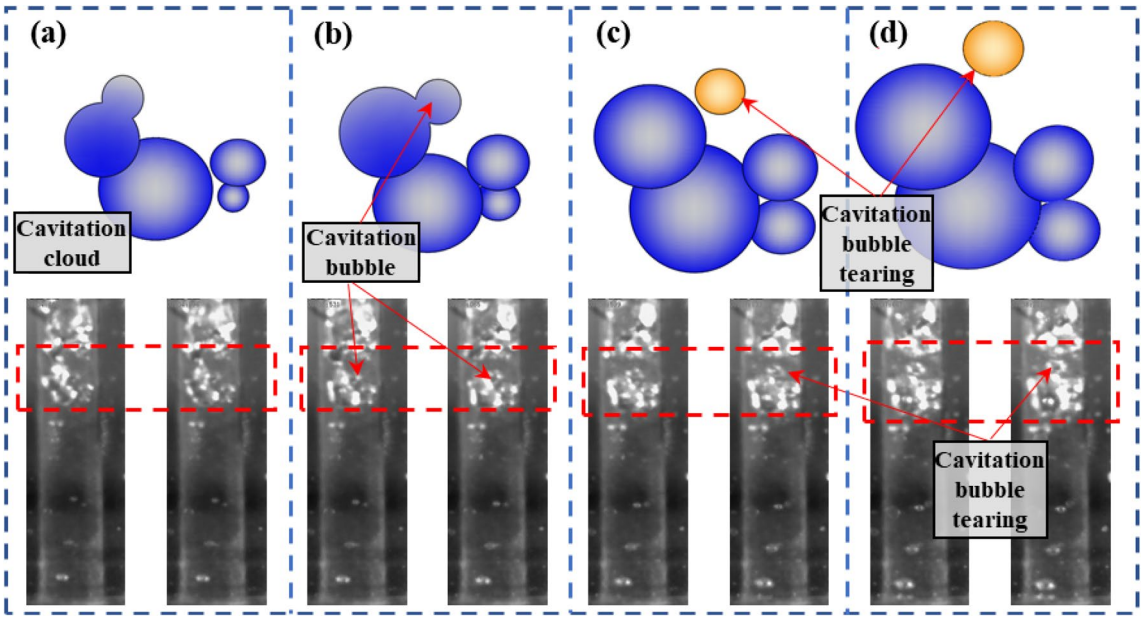

Figure 11 Diagram of cavitation bubbles development

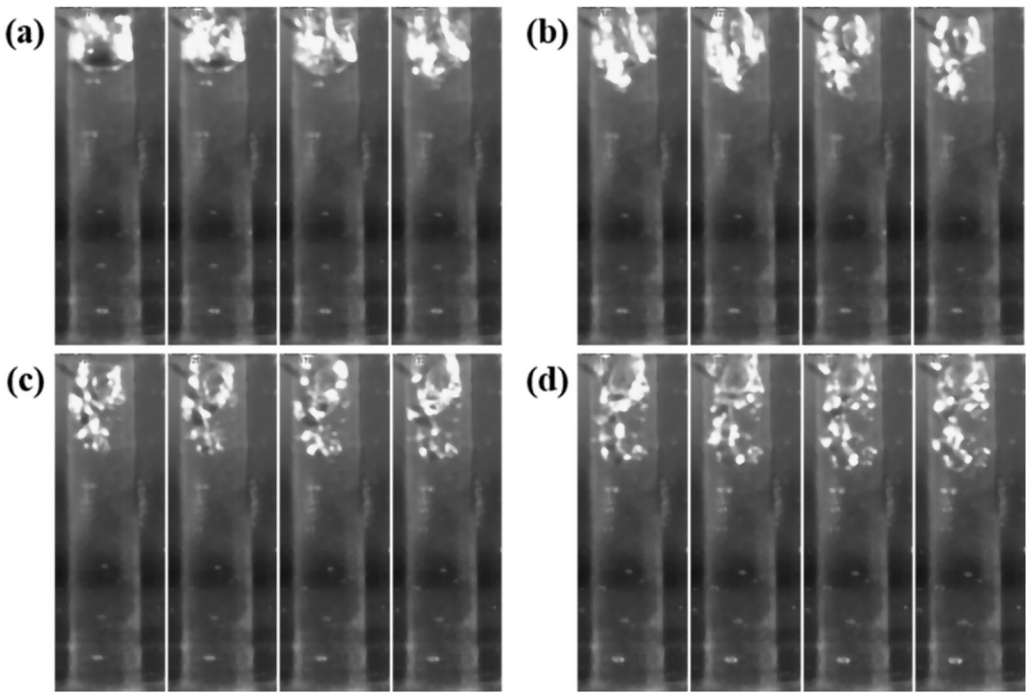

Figure 12 Diagram of cavitation bubbles collapse

the gas in the container, the gas will turn back into liquid under high pressure). Therefore, in the VAC process, the formation and collapse of cavitation bubbles is a cyclic process, corresponding to a volume alternating process.

4.4 Discussion

In the condition of an ideal gas, it can be assumed that P^*V/T is constant in an airtight container. Hence, P is inversely proportional to V when the temperature is constant, i.e., the pressure inside the airtight container

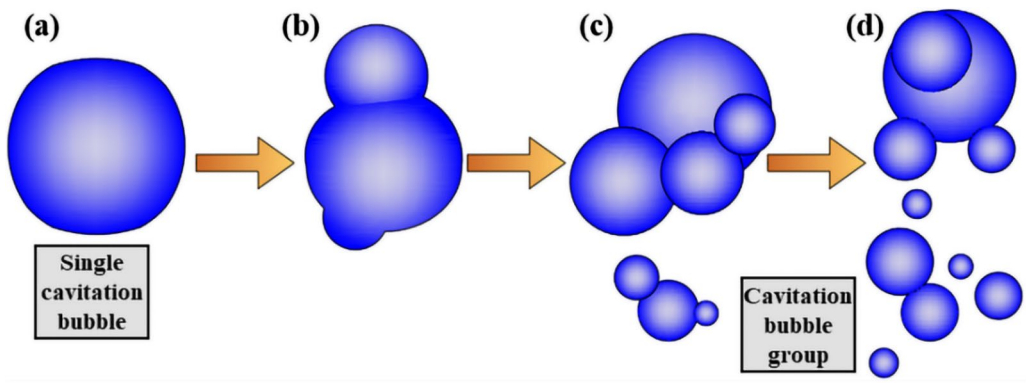

Figure 13 Schematic diagram of cavitation bubble collapse

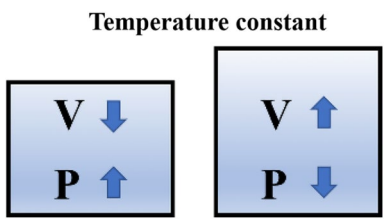

Figure 14 *V*, *P* diagram with the Temperature constant in an airtight container

decreases as the airtight container volume increases. When the volume increases to a certain extent, the pressure P must be less than the saturated vapor pressure of the liquid. Therefore, the liquid inside the container is going to be converted into a gas. Meanwhile, when the volume decreases, the gas turns into a liquid. Here, P denotes the pressure in the airtight container, V denotes the volume in the airtight container, and T denotes the temperature in the airtight container. Figure 14 is the V, P diagram with the Temperature constant in an airtight container.

In the airtight container, the gas and liquid are cyclically converted, corresponding to the formation and collapse of cavitation bubbles, such as the cavitation phenomenon photographed by the high-speed camera. The comparison of simulation and experiment in this paper illustrates the formation position and evolution of cavitation bubbles in the VAC process, which is essentially the feasibility analysis of VAC. It proves that cavitation bubbles can be generated in liquid by volume alternation. The comparison between simulation and experiment explains the formation position and evolution process of cavitation bubbles, which provides strong proof for the feasibility of VAC. The results indicate that simulation and experiment have obvious consistency in terms of the formation position and evolution law of cavitation bubbles.

Compared with the traditional method of indirectly generating low pressure by exploiting the velocity difference in water, this study directly constructs a low-pressure environment similar to a vacuum, which is a completely new cavitation generation method.

5 Conclusions

In this study, numerical simulation and experimental analysis of VAC were conducted, and the following conclusions were drawn.

(1) VAC is feasible as a new cavitation generation method. The whole experiment and simulation are based on the premise that the piston moving frequency is 18 Hz and the piston moving stroke is 20 mm to realize the alternate changes of volume. In the initial stage when the volume begins to increase, cavitation bubbles constantly form at the bottom of the container, and there is a large number of cavitation bubbles, at the upper surface, so this stage can be regarded as the cavitation bubble formation stage. As the volume continues to increase, the cavitation cloud separation phenomenon occurs, and other small bubbles are generated in the separation process, so this stage can be regarded as the development stage of the cavitation cloud. Finally, when the volume returns to its original size, the cavitation collapse stage occurs.

(2) As a new cavitation generation method, VAC needs to be further studied. The position of generating cavitation and the law of cavitation evolution have been studied. Subsequent studies can include piston motion frequency, piston motion stroke, different liquid phases and other aspects.

(3) The study of VAC has significant research significance and paves the way for its application in the industry in the future, such as, accurate polishing of

complex microcavity, rapid manufacturing of emulsion, cavitation cleaning and so on, etc.

Acknowledgements
The authors sincerely thanks to Professor Ruitao Li of Jiangsu University for his critical discussion and reading during manuscript preparation.

Author Contributions
SC was in charge of the conceptualization, methodology, validation, formal analysis and visualization. YW was in charge of the methodology, validation, methodology, formal analysis and funding acquisition. FL, SX was in charge of the sampling and laboratory analyses, project administration. ZX, CY, KZ assisted with resources and supervision. All authors read and approved the final manuscript.

Authors' Information
Shangshuang Chen, born in 1996, is currently an engineer at *Positec Technology Company, Ltd., China*. He received his master's degree from *Jiangsu University, China*, in 2022. His research interests include surface treatment and special processing.
Yun Wang, born in 1975, is currently a Professor at *Jiangsu University, China*. His research interests include micro-forming technology, cavitation water jet, high-precision, etc.
Fuzhu Li, born in 1971, is currently a Professor at *Jiangsu University, China*. His research interests include electromechanical hydraulic integration system and cavitation technology.

Funding
Supported by National Nature Science Foundation of China (Grant No. 51575245), Jiangsu Provincial Key research and development program (Grant No. BE2015134), Zhenjiang Municipal Key Research and Development Project (Grant No. KZ2020001).

Data availability statement
The data that support the findings of this study are available from the corresponding author upon reasonable request.

Declarations

Competing Interests
The authors declare no competing financial interests.

Received: 7 December 2021 Revised: 24 April 2023 Accepted: 4 May 2023
Published online: 30 May 2023

References

[1] A Sarc, T Stepisnik-Perdih, M Petkovsek, et al. The issue of cavitation number value in studies of water treatment by hydrodynamic cavitation. *Ultrason Sonochem*, 2017, 34: 51–59.
[2] N Fujisawa, T Kikuchi, K Fujisawa, et al. Time-resolved observations of pit formation and cloud behavior in cavitating jet. *Wear*, 2017, 386–387: 99–105.
[3] A P Nagalingam, V C Thiruchelvam, S H Yeo. A novel hydrodynamic cavitation abrasive technique for internal surface finishing. *Journal of Manufacturing Processes*, 2019, 46: 44–58.
[4] X Sun, J Liu, L Ji, et al. A review on hydrodynamic cavitation disinfection: The current state of knowledge. *Sci Total Environ*, 2020, 737: 139–606.
[5] P Thanekar, P R Gogate, Z Znak, et al. Degradation of benzene present in wastewater using hydrodynamic cavitation in combination with air. *Ultrason Sonochem*, 2020, 70: 105–296.
[6] D Panda, V K Saharan, S Manickam. Controlled hydrodynamic cavitation: A review of recent advances and perspectives for greener processing. *Processes*, 2020: 8.
[7] M Petkovsek, M Dular. Cavitation dynamics in water at elevated temperatures and in liquid nitrogen at an ultrasonic horn tip. *Ultrason Sonochem*, 2019, 58: 104652.
[8] J Cui, Z Zhang, X Liu, et al. Analysis of the viscosity reduction of crude oil with nano-Ni catalyst by acoustic cavitation. *Fuel*, 2020: 275.
[9] Z Shen, J Shao, J Zhang, et al. Ultrasound cavitation enhanced chemotherapy: In vivo research and clinical application. *Experimental Biology and Medicine*, 2020, 245: 1200–1212.
[10] A Priyadarshi, M Khavari, T Subroto, et al. On the governing fragmentation mechanism of primary intermetallics by induced cavitation. *Ultrason Sonochem*, 2020, 70: 105–260.
[11] Y Zhang, X Qiu, X Zhang, et al. Collapsing dynamics of a laser-induced cavitation bubble near the edge of a rigid wall. *Ultrason Sonochem*, 2020, 67: 105–157.
[12] Y Zhang, X Xie, Y Zhang, et al. Experimental study of influences of a particle on the collapsing dynamics of a laser-induced cavitation bubble near a solid wall. *Experimental Thermal and Fluid Science*, 2019, 105: 289–306.
[13] P Alfonso-Muniozguren, M Hazzwan Bohari, A Sicilia, et al. Tertiary treatment of real abattoir wastewater using combined acoustic cavitation and ozonation. *Ultrasonics Sonochemistry*, 2020, 64: 104–986.
[14] J Sáez-Bastante, M Carmona-Cabello, S Pinzi, et al. Recycling of kebab restoration grease for bioenergy production through acoustic cavitation. *Renewable Energy*, 2020, 155: 1147–1155.
[15] X Sun, X Xuan, Y Song, et al. Experimental and numerical studies on the cavitation in an advanced rotational hydrodynamic cavitation reactor for water treatment. *Ultrason Sonochem*, 2021, 70: 105–311.
[16] J Kosel, A Sinkovec, M Dular. A novel rotation generator of hydrodynamic cavitation for the fibrillation of long conifer fibers in paper production. *Ultrason Sonochem*, 2019, 59: 104–721.
[17] J Kosel, M Sustarsic, M Petkovsek, et al. Application of (super)cavitation for the recycling of process waters in paper producing industry. *Ultrason Sonochem*, 2020, 64: 105002.
[18] F Chen, H Wang, Y Tang, et al. Novel cavitation fluid jet polishing process based on negative pressure effects. *Ultrason Sonochem*, 2018, 42: 339–346.
[19] F Chen, H Wang, S Yin, et al. Cavitation water-suction polishing of metallic materials under negative-pressure effect. *Journal of Materials Processing Technology*, 2019, 273: 116–257.
[20] A Lu, Z Shang, X Luo, et al. Rapid fabrication of ultra-smooth Y-TZP bioceramic surfaces by dual-axis wheel polishing: process development and tribological characterization. *Journal of Manufacturing Processes*, 2020, 55: 276–287.
[21] K L Tan, S H Yeo. Bubble dynamics and cavitation intensity in milliscale channels under an ultrasonic horn. *Ultrason Sonochem*, 2019, 58: 104–666.
[22] Y Zhang, F Chen, Y Zhang, et al. Experimental investigations of interactions between a laser-induced cavitation bubble and a spherical particle. *Experimental Thermal and Fluid Science*, 2018, 98: 645–661.
[23] M Kauer, V Belova-Magri, C Cairos, et al. Visualization and optimization of cavitation activity at a solid surface in high frequency ultrasound fields. *Ultrason Sonochem*, 2017, 34: 474–483.
[24] F Li. Study on dynamic evolution of cavitation clouds and optimization of standoff distance in water cavitation peening. *Journal of Mechanical Engineering*, 2019, 55(9): 120–126.
[25] S Q Cai. Cavitation occurring in capillary tubes. *Physics Letters A*, 2019, 383: 509–513.
[26] K Babina, M Polyakova, I Sokhova, et al. The effect of finishing and polishing sequences on the surface roughness of three different nanocomposites and composite/enamel and composite/cementum interfaces. *Nanomaterials (Basel)*, 2020, 10: 1007–1339.
[27] Hemant J Sagar, Ould el Moctar. Dynamics of a cavitation bubble near a solid surface and the induced damage. *Journal of Fluids and Structures* 2020, 92: 102–799.
[28] T N Chen, Z N Guo, B W Zeng, et al. Experimental research and numerical simulation of the punch forming of aluminum foil based on a laser-induced cavitation bubble. *The International Journal of Advanced Manufacturing Technology*, 2017, 93: 3275–3284.
[29] L Cheng, J Li, X Xue, et al. Effect of β/B2 phase on cavitation behavior during superplastic deformation of TiAl alloys. *Journal of Alloys and Compounds*, 2017, 693: 749–759.

[30] H Soyama, F Takeo. Comparison between cavitation peening and shot peening for extending the fatigue life of a duralumin plate with a hole. *Journal of Materials Processing Technology*, 2016, 227: 80–87.
[31] Q N Song, N Xu, Y F Bao, et al. Corrosion and cavitation erosion behaviors of two marine propeller materials in clean and sulfide-polluted 3.5% NaCl solutions. *Acta Metallurgica Sinica (English Letters)*, 2017, 30: 712–720.
[32] F Reuter, R Mettin. Mechanisms of single bubble cleaning. *Ultrason Sonochem*, 2016, 90: 550–562.
[33] J Zhou, X Niu, C Yang, et al. Surface action mechanism and planarization effect of sarcosine as an auxiliary complexing agent in copper film chemical mechanical polishing. *Applied Surface Science*, 2020, 529: 109–147.